Colloids and Surfaces B: Biointerfaces 146 (2016) 188–197

Contents lists available at ScienceDirect

Colloids and Surfaces B: Biointerfaces

journal homepage: www.elsevier.com/locate/colsurfb

Transcutaneous iontophoretic delivery of STAT3 siRNA using layer-by-layer chitosan coated gold nanoparticles to treat melanoma

Suman Labala, Anup Jose, Venkata Vamsi Krishna Venuganti*

Department of Pharmacy, Birla Institute of Technology and Science (BITS) Pilani, Hyderabad Campus, Shameerpet, Hyderabad 500078, India

ARTICLE INFO

Article history:
Received 26 January 2016
Received in revised form 19 May 2016
Accepted 26 May 2016
Available online 3 June 2016

Keywords:
Layer-by-layer assembly
Gold nanoparticles
STAT3 siRNA
Melanoma
Chitosan
B16F10 cells
Skin penetration

ABSTRACT

Overexpression of signal transducer and activator of transcription 3 (STAT3) protein prevents apoptosis and enhances proliferation of melanocytes. The aim of this study was to investigate the feasibility of using layer-by-layer assembled gold nanoparticles (LbL-AuNP) as a carrier for iontophoretic delivery of STAT3 siRNA to treat melanoma. Chitosan coated AuNP (AuNP-CS) were prepared by direct reduction of $HAuCl_4$ in the presence of chitosan. The AuNP-CS were then sequentially layered with siRNA and chitosan to form AuNP-CS/siRNA/CS. STAT3 siRNA replaced with scrambled siRNA or sodium alginate were used as controls. The average particle size and zeta-potential of the prepared LbL-AuNP were 150 ± 10 nm (PDI: 0.41 ± 0.06) and 35 ± 6 mV, respectively. *In vitro* studies in B16F10 murine melanoma cells showed that AuNP-CS/siRNA/CS inhibited the cell growth by $49.0 \pm 0.6\%$ and $66.0 \pm 0.2\%$ at 0.25 nM and 0.5 nM STAT3 siRNA concentration, respectively. Fluorescence microscopy and flow cytometry studies showed a time dependent cell uptake of the LbL-AuNP up to 120 min. Clathrin mediated endocytosis was found to be the predominant cell uptake mechanism for LbL-AuNP. STAT3 siRNA loaded LbL-AuNP reduced the STAT3 protein expression by 47.3% in B16F10 cells. Similarly, apoptosis assay showed 29% and 44% of early and late apoptotic events, respectively after treatment with STAT3 siRNA loaded LbL-AuNP. Confocal microscope and skin cryosections showed that application of 0.47 mA/cm^2 of anodal iontophoresis enhanced the skin penetration of LbL-AuNP to reach viable epidermis. In conclusion, layer-by-layer chitosan coated AuNP can be developed as a carrier for iontophoretic delivery of STAT3 siRNA to treat melanoma.

1. Introduction

Melanoma is a malignant skin cancer associated with the melanocytes in epidermis. A worldwide melanoma incidence in 2012 included 232,000 new cases and 55,000 deaths [1]. The current treatment options available against melanoma include surgical resection of the tumor, followed by radiation or chemotherapy. Small molecule chemotherapeutic agents clinically available against melanoma include dacarbazine, cisplatin, and more recently approved dabrafenib [2]. Furthermore, monoclonal antibodies and immunomodulators are being investigated in various clinical trials [3]. A serine-threonine protein kinase, BRAF has been one of the key targets investigated to control melanoma progression [4]. Multiple chemotherapeutic agents including vemurafenib and dabrafenib target a mutated form of BRAF (BRAFV600E) [5,6]. However, it has been identified that inhibition of BRAF did not completely regress the tumor and the cancer cells developed resistance towards the BRAF inhibitors [7]. Meanwhile, signal transducer and activator of transcription 3 (STAT3) is an intracellular signaling molecule implicated in the survival, proliferation, angiogenesis, metastasis and immune evasion of cancer cells [8]. STAT3 has been reported to be overexpressed in multiple cancer types including melanoma [8,9]. It has been shown that inhibition of STAT3 down regulates genes involved in angiogenesis and metastasis and promotes apoptosis of cancer cells [10]. However, there have been no small molecule inhibitors of STAT3 protein reported. To that end, STAT3 protein suppression using RNA interference mechanism holds promise [10]. Here, we report the growth inhibition of melanoma using anti-STAT3 small interfering RNA (siRNA).

siRNA suppresses unwanted protein production by binding to target mRNA in a sequence specific manner and preventing the mRNA translation to protein [11]. However, the clinical application of therapeutic siRNA is limited by its poor deliverability. siRNA is highly prone to degradation by nucleases resulting in short half-

* Corresponding author at: Department of Pharmacy, BITS Pilani, Hyderabad Campus, Shameerpet, Hyderabad 500078, Telangana, India.
E-mail addresses: vamsi@hyderabad.bits-pilani.ac.in, vamsi.venuganti@gmail.com (V.V.K. Venuganti).

http://dx.doi.org/10.1016/j.colsurfb.2016.05.076
0927-7765/

life [12]. Furthermore, siRNA shows poor penetration across the biological barriers including epithelial, endosomal, and cell membrane barrier [12]. To overcome the siRNA delivery challenges, non-viral nucleic acid carriers have been developed [13]. These include liposomes and polymeric nanoparticles among others. In general, cationic polymers or lipidic systems are complexed to negatively charged siRNA through electrostatic interactions [13]. The overall positive charge and nanoscale particle size of the carrier-siRNA complex helps in its translocation across biomembranes to reach intracellular compartments [14,15].

Recently, metal-based nanoparticles such as gold nanoparticles have shown potential in biomedical applications including imaging, drug delivery and photothermal therapy [16,17]. This is attributed to their biocompatibility, chemically inert property, nanosize, possibility to attach various ligands for targeting and longer plasma circulation [18,19]. In our earlier report, we have presented that layer-by-layer polymer coated gold nanoparticles were stable in various ionic media including cell culture medium [20]. These blank layer-by-layer gold nanoparticles prepared by alternative adsorption of polyethylenimine and polystyrene sulfonate were found to show cytotoxicity in B16F10 murine melanoma cells. The cytotoxicity was attributed to the outer layer of polyethylenimine [21]. In this study, we replaced the polyethylenimine with low molecular weight chitosan to reduce the toxicity of blank layer-by-layer gold nanoparticles. Chitosan is a naturally occurring biodegradable polysaccharide obtained through deacetylation of chitin [22]. The low molecular weight chitosan has been reported to show minimal cytotoxicity compared to high molecular weight chitosan [23]. Here, we have constructed layer-by-layer gold nanoparticle as a carrier for siRNA by sequential adsorption of chitosan and siRNA.

To deliver the STAT3 siRNA against melanoma in a non-invasive fashion, the siRNA loaded gold nanoparticles were topically applied. To improve the skin penetration of gold nanoparticles, a physical penetration enhancement technique, iontophoresis was employed. We hypothesized that iontophoresis would enhance the skin penetration of siRNA entrapped nanoparticles, and cationic nanoparticles themselves would be rapidly taken up by the cancer cells through endocytosis mechanisms. The cell uptake mechanism was studied by inhibiting clathrin and caveolea mediated endocytosis pathways.

2. Materials and methods

2.1. Materials

Tetrachloroaurate trihydrate ($HAuCl_4$ $3H_2O$), sodium alginate (SA, MW: 40 kDa), poly(N-vinyl pyrrolidone) (PVP K-30, MW: 40 kDa), fluorescein isothiocyanate (FITC), Triton X-100, DAPI, and nitrocellulose membrane were purchased from Sigma Aldrich Chemical Company (Bengaluru, India). Chitosan (CS, MW: 15 kDa, degree of deacetylation: 85%) was purchased from Polysciences Inc., USA. STAT3 siRNA (sense: 5′-AAAUGAAGGUGGUGGAGAAUU-3′; anti-sense: 5′-UUCUCCACCACCUUCAUUUUU-3′) was purchased from Dharmacon Inc., USA. Scrambled sequence siRNA, STAT3 monoclonal antibody, β-actin primary antibody and horseradish peroxidase-conjugated secondary antibodies were purchased from Santa Cruz Biotechnology Inc., USA. Silencer® Cy™3 labeled siRNA was purchased from Life Technologies Inc., USA. Dulbecco's modified Eagle's medium (DMEM), Dulbecco's phosphate buffered saline, fetal bovine serum (FBS) and thiazolyl blue tetrazolium bromide (MTT) were purchased from Himedia Laboratories (Mumbai, India). All the chemicals were used without further purification. Milli-Q (Millipore Corporation, USA) water with resistivity of 18.2 MΩ cm^{-1} was used for all the experiments.

2.2. Preparation of chitosan capped gold nanoparticles (AuNP-CS)

Chitosan capped gold nanoparticles (AuNP-CS) were prepared by direct reduction of $HAuCl_4$ using chitosan. $HAuCl_4$ (0.25 mM) was mixed with chitosan solution and heated at 100 °C. This reaction mixture was allowed to boil under continuous agitation until the color turns deep red indicating formation of AuNP [24,25]. To optimize the $HAuCl_4$ reduction, different concentrations of chitosan (0.1–0.5% w/w) were studied. Later, PVP was added as a stabilizing agent at 60:1 molar ratio (PVP monomer/$HAuCl_4$). For this, aqueous solution of PVP was added drop wise to AuNP-CS solution and the reaction mixture was stirred at 1200 rpm for 24 h. The AuNP-CS particles were further used for adsorption of siRNA.

2.3. Layer-by-layer adsorption of siRNA and CS on AuNP-CS

The optimal nitrogen to a phosphate (N/P) ratio of AuNP-CS and siRNA for complexation was determined by gel retardation assay. siRNA (1 nM) in HEPES buffer (10 mM) was mixed with AuNP-CS at 5:1 and 10:1 w/w ratio and incubated for 2 h. Later, the sample was centrifuged at 15,000 rpm for 30 min to remove unadsorbed siRNA. The supernatant (10 μl) was mixed with 2 μl of 6X loading buffer (10 mM Tris-HCl, 0.03% bromophenol blue, 0.03% xylene cyanol FF, 60% glycerol, 60 mM EDTA). Electrophoresis was performed using 2% agarose gel in a horizontal gel electrophoresis unit (Bio-Rad Laboratories, USA) ran at 50 V for 2 h. Then the bands were stained with 0.5 μg/ml ethidium bromide for 10 min and visualized using a gel documentation system (Gel Doc XR+ Imaging system, Bio-Rad Laboratories, USA). The gel retardation assay showed that 10:1 (AuNP/siRNA) ratio resulted in greater complexation. Then the AuNP-CS/siRNA particles were coated with CS. For this, the AuNP-CS/siRNA particles were incubated with chitosan solution (1 mg/ml) for 1 h under continuous stirring at 1200 rpm to form AuNP-CS/siRNA/CS nanoparticles. The encapsulation efficiency (EE) of siRNA was determined by measuring the absorbance of the supernatant collected during deposition and washing steps at 260 nm wavelength using biospectrometer® (Eppendorf, Germany). The EE of siRNA was calculated using Eq. (1)

$$\text{Encapsulation efficiency (\%)} = \frac{\text{Total amount of siRNA} - \text{amount of siRNA in supernatant}}{\text{Total amount of siRNA}} \times 100 \quad (1)$$

As control nanoparticle formulations, LbL-AuNP were prepared by replacing STAT3 siRNA with scrambled siRNA or sodium alginate (SA). LbL-AuNP prepared by replacing siRNA with SA was used to study the effect of blank LbL-AuNP on cell viability and apoptosis potential.

2.4. Effect of STAT3 siRNA on melanocyte cell viability

B16F10 murine melanoma cells were cultured in a growth medium containing Dulbecco's modified Eagle's medium (DMEM) supplemented with 10% fetal bovine serum (FBS) and 1% penicillin/streptomycin solution. Cells were incubated at 37 °C and 5% CO_2. For cell viability study, cells (1×10^4) were seeded in a 96-well plate 24 h before incubation with formulations. Cell viability was studied at different concentrations of AuNP-CS and AuNP-CS/STAT3 siRNA/CS. Nanoparticles loaded with scrambled siRNA or SA were used as negative control and particle size control, respectively.

Formulations were prepared in DMEM at siRNA concentration of 0.25 nM and 0.5 nM. Free STAT3 siRNA was used at 0.5 nM concentration. AuNP-CS and AuNP-CS/SA/CS were studied at Au concentration of 338 μM and 675 μM. The cells were incubated with formulations for 8 h at 37 °C. Later, the culture medium was replaced with fresh medium and cells were further incubated for

48 h. Then the cell viability was determined using MTT assay, where the absorbance of DMSO solubilized formazan crystals was measured at 572 nm wavelength [20].

2.5. Cell uptake studies

Cell uptake studies were performed using AuNP-CS/SA/CS in B16F10 cells. To visualize nanoparticles using fluorescence microscope, CS was labeled with FITC as described in the Supplementary material. B16F10 cells (1×10^5) were seeded in a 12-well plate and incubated at 37 °C. After 24 h, cells were treated with FITC labeled AuNP-CS/SA/CS for 15, 30, 60 and 120 min. Later, cells were washed with ice cold PBS and fixed using 4% paraformaldehyde. Cells were permeabilized using 0.1% Triton X-100 and incubated with DAPI (1 μg/ml) for 5 min. Fluorescence images were acquired after excitation of FITC and DAPI at 488 and 358 nm wavelength, respectively using 20X objective lens (Olympus IX53, Olympus Corporation, Japan). Image analyses were performed using Image J software (version 1.47 V, National Institutes of Health, USA).

2.6. In vitro *gene silencing*

In vitro gene silencing of STAT3 siRNA delivered using LbL-AuNP was performed by Western blot analysis. B16F10 cells (2×10^5) were seeded in a 6-well plate and treated for 8 h with AuNP-CS/STAT3 siRNA/CS, AuNP-CS/scrambled siRNA/CS containing 0.25 or 0.5 nM siRNA. AuNP-CS/SA/CS was used as size control at Au concentration of 338 μM and 675 μM. After incubation, the unentrapped formulation was removed and replaced with cell culture medium containing DMEM supplemented with 10% FBS and further incubated for 48 h at 37 °C. Later, the Western blot analysis was performed as described in the Supplementary information.

2.7. Apoptosis assay

The induction of apoptosis by siRNA loaded AuNP was studied using FITC-Annexin V/PI apoptosis assay (Molecular Probes, Inc, USA). B16F10 cells (2×10^5) were seeded in a 6-well plate and treated for 8 h with AuNP-CS/STAT3 siRNA/CS, AuNP-CS/scrambled siRNA/CS at 0.25 and 0.5 nM siRNA concentration.

For flow cytometric analysis, the cells were harvested using trypsin and suspended in ice cold PBS. The cell count was determined by trypan blue exclusion assay. The cells were centrifuged at 1200 rpm for 5 min and the cell pellet was resuspended in 1X annexin binding buffer (5 mM HEPES, 140 mM NaCl, 2.5 mM $CaCl_2$, pH 7.4). FITC-Annexin V (5 μl) and 1 μl of 100 μg/ml propidium iodide solutions were added to each of 100 μl cell suspension and incubated for 15 min at room temperature. After the incubation period, 400 μl of 1X annexin binding buffer was added. The fluorescence intensity of FITC and PI were measured at 530 nm and 575 nm emission wavelength, respectively. The cell population (%) was separated into four groups; live cells (no fluorescence, Annexin V−/PI−); early apoptotic cells (green fluorescence, Annexin V+/PI−); late apoptotic cells (both green and red fluorescence, Annexin V+/PI+) and dead cells (red fluorescence, Annexin V−/PI+).

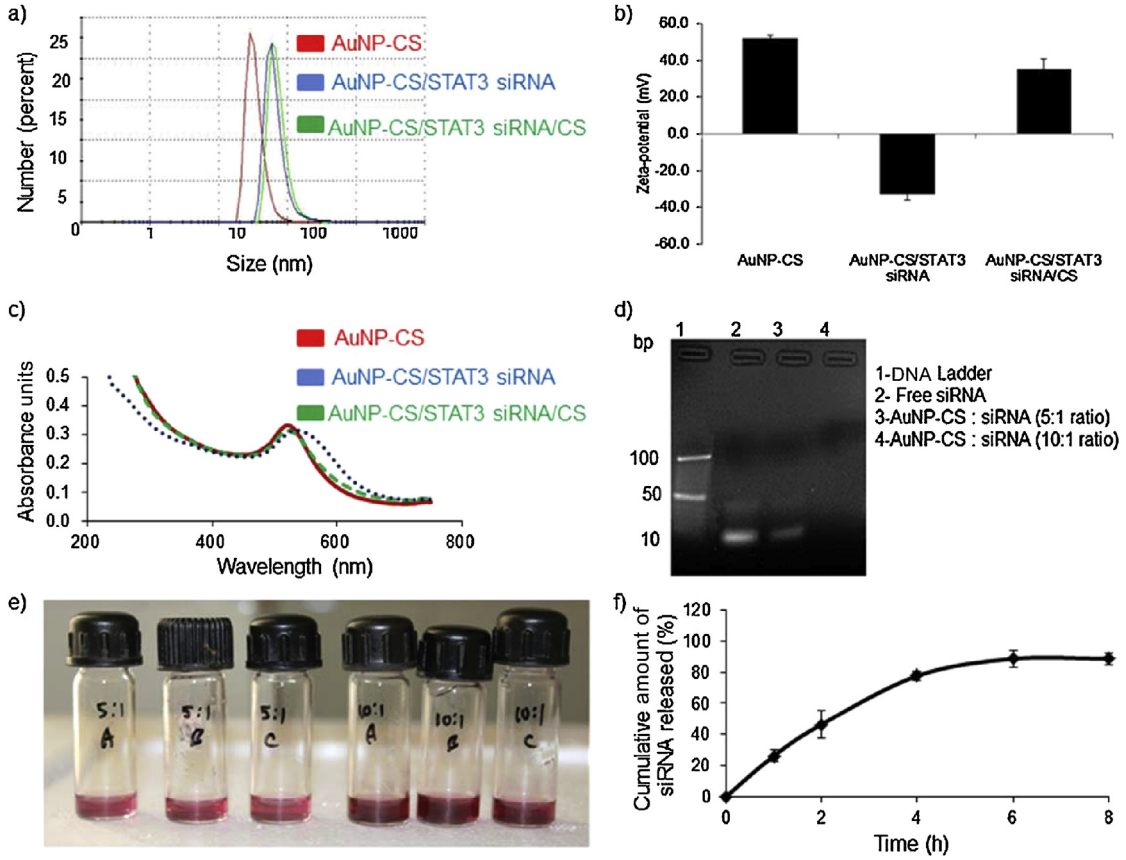

Fig. 1. Characterization of chitosan functionalized gold nanoparticles. (a) Representative number weighted particle size distribution after sequential adsorption of siRNA and chitosan on AuNP-CS; (b) zeta-potential measured after sequential adsorption of siRNA and chitosan on AuNP-CS; (c) surface plasmon resonance upon sequential adsorption of chitosan, siRNA and chitosan up on AuNP; (d) optimization of the CS-AuNP and siRNA complex weight ratio (w/w) using agarose gel retardation assay; (e) digital photograph of LbL-AuNP-CS/siRNA/CS prepared at 5:1 and 10:1 (N/P) ratios; (f) cumulative percentage of siRNA released from LbL-AuNP with time. Data in (b) and (f) was presented as mean (n = 3) ± standard deviation.

2.8. Skin penetration of siRNA loaded lbL-AuNP

Skin penetration of Cy3 labeled siRNA was performed using excised porcine ear skin. The skin sample preparation method was described in Supplementary material.

Excised skin sample was mounted between receptor and donor compartments of a Franz diffusion cell (Permegear Inc., USA) with stratum corneum (SC) facing the donor compartment. The effective diffusional area was 0.637 cm^2 and the volume of receptor compartment was 5 ml. PBS (pH 7.4) was used as receptor medium and maintained at 37 ± 0.5 °C. Cy3 labeled siRNA and FITC labeled CS were used to construct AuNP-CS/siRNA/CS. The donor compartment was charged with AuNP-CS/siRNA/CS dispersed in 0.2 ml of PBS (pH 7.4). For anodal iontophoresis application, a current density of 0.47 mA/cm^2 was applied for 4 h using silver electrode placed in the donor and silver chloride electrode placed in the receptor compartment. A salt bridge (1% agarose containing 2 mM NaCl) was used to avoid direct contact of silver wire with formulation. After 4 h passive or iontophoretic treatment, the skin samples were analyzed using confocal laser scanning microscope and skin cryosections as described in Supplementary material.

2.9. Statistical analysis

All the results were presented as mean ± standard deviation. The results were compared by performing analysis of variance (GraphPad Prism V6, USA), and the results were considered to be significant at $p < 0.05$.

3. Results

3.1. Characterization of the layer-by-layer AuNP

The methodology for characterization studies was presented in Supplementary material. Fig. 1ashows that the particle size increased from 62.5 ± 3.4 nm (PDI: 0.27 ± 0.04) to 83.1 ± 7.4 nm (PDI: 0.27 ± 0.08) and 150.4 ± 10.1 nm (PDI: 0.41 ± 0.06) after LbL adsorption of STAT3 siRNA and CS, respectively. The zeta-potential was found to be (−)32.7 ± 3.1 mV and +35.1 ± 5.8 mV after adsorption of STAT3 siRNA and CS, respectively (Fig. 1b). LbL adsorption of STAT3 siRNA and CS onto CS-AuNP showed bathochromic shift in plasmonic peak wavelength at 524 nm and 530 nm, respectively from the initial 521 nm wavelength (Fig. 1c). Table 1 shows the average particle size, zeta-potential and plasmonic peak after sequential adsorption of CS and siRNA. There was no significant difference in the particle size, zeta-potential and plasmonic peak wavelength among the nanoparticles prepared using STAT3 siRNA or scrambled siRNA (Table 1). On the other hand, when siRNA is replaced with SA, the particle size increased to 162.6 ± 3.6 nm (PDI: 0.28 ± 0.02) and after adsorption of CS, the particle size increased to 172.7 ± 8.8 nm (PDI: 0.35 ± 0.03). Similarly, the zeta-potential was found to be (−)76.6 ± 3.3 mV and +41.1 ± 1.1 mV after adsorption of SA and CS on AuNP-CS. Fig. 1e shows the digital photograph of AuNP-CS/siRNA/CS prepared at 5:1 and 10:1 (N/P) ratio. Fig. 1f shows the *in vitro* release of siRNA from LbL-AuNP dispersed in phosphate buffer (7.4). The complete release of siRNA from LbL-AuNP was achieved after 6 h incubation.

Table S1 (Supplementary) shows the stability of AuNP-CS after incubation in PBS and cell culture medium at different time points. The particle size of AuNP-CS increased from 62.5 ± 3.4 nm (PDI: 0.27 ± 0.04) to 162.0 ± 4.8 nm (PDI: 0.20 ± 0.02) and 228.8 ± 11.8 nm (PDI: 0.23 ± 0.02) after incubation in PBS and DMEM for 48 h, respectively. The zeta-potential was neutralized and no significant increase in plasmonic peak wavelength was observed.

Table S2 (Supplementary) shows the stability of AuNP-CS/siRNA/CS incubated in PBS or DMEM up to 72 h. The AuNP-CS/siRNA/CS particles were stable without significant change in particle size, zeta-potential and plasmonic peak wavelength for up to 48 h. Further incubation up to 72 h increased the particle size to 203.6 ± 16.3 nm (PDI: 0.38 ± 0.01), decreased the zeta-potential to −2.9 ± 1.0 mV.

UV-spectrophotometer analysis showed that the encapsulation efficiency of siRNA was 21.6 ± 5.7% and 58.3 ± 7.5% at AuNP-CS to siRNA ratio of 5:1 and 10:1, respectively. This translates to approximately 3×10^3 and 8×10^3 molecules of siRNA adsorbed to one AuNP-CS nanoparticle at 5:1 and 10:1 w/w ratio, respectively.

3.2. Cell uptake studies

Cell uptake studies were performed using FITC labeled AuNP-CS/SA/CS. FITC labeling of chitosan was confirmed by thin layer chromatography. FITC conjugation of chitosan resulted in a shift in absorption maxima of FITC from 491 nm to 495 nm wavelength. Spectrofluorimetry showed peak emission wavelength at 519 nm and 522 nm for free FITC and FITC-chitosan, respectively. Supplementary Fig. S2 shows FTIR spectra of free FITC and FITC-chitosan conjugate. UV–vis spectroscopic analysis showed 0.28 mol of FITC conjugated to one mole of chitosan.

Fig. 2ashows the fluorescence images of B16F10 cells after incubation with FITC labeled AuNP-CS/SA/CS for 15, 30, 60 and 120 min. After 15 min of incubation, fluorescence images suggest that the LbL-AuNP were taken up in B16F10 cells. Background corrected fluorescence image analysis showed a gradual increase in cell associated fluorescence with the increase in incubation time from 15 min to 120 min (Fig. 2b). After 60 min incubation, FITC labeled LbL-AuNP were completely associated with B16F10 cells as observed from merged images.

Table 1
Particle size, zeta-potential and plasmon resonance wavelength of siRNA loaded LbL-AuNP.

Nanoparticle	Particle size (nm)[a]	Zeta-potential (mV)	Plasmonic peak (nm)
STAT3 siRNA			
AuNP-CS	62.5 ± 3.4 (0.27 ± 0.04)	52.1 ± 1.7	520
AuNP-CS/STAT3 siRNA	83.1 ± 7.4 (0.27 ± 0.08)	−32.7 ± 3.1	524
AuNP-CS/STAT3 siRNA/CS	150.4 ± 10.1 (0.41 ± 0.06)	35.1 ± 5.8	530
Scrambled siRNA			
AuNP-CS	62.5 ± 3.4 (0.27 ± 0.04)	52.1 ± 1.7	520
AuNP-CS/Scrambled siRNA	79.7 ± 8.5 (0.35 ± 0.12)	−28.5 ± 0.6	524
AuNP-CS/Scrambled siRNA/CS	157.3 ± 19.1 (0.28 ± 0.04)	31.9 ± 0.5	530
Sodium alginate (SA)			
AuNP-CS	62.5 ± 3.4 (0.27 ± 0.04)	52.1 ± 1.7	520
AuNP-CS/SA	162.6 ± 3.6 (0.28 ± 0.02)	−76.6 ± 3.3	526
AuNP-CS/SA/CS	172.7 ± 8.8 (0.35 ± 0.03)	41.1 ± 1.1	532

Data are presented as mean ± standard deviation (n = 3).
[a] Values in parentheses represent polydispersity index (PDI) ± standard deviation.

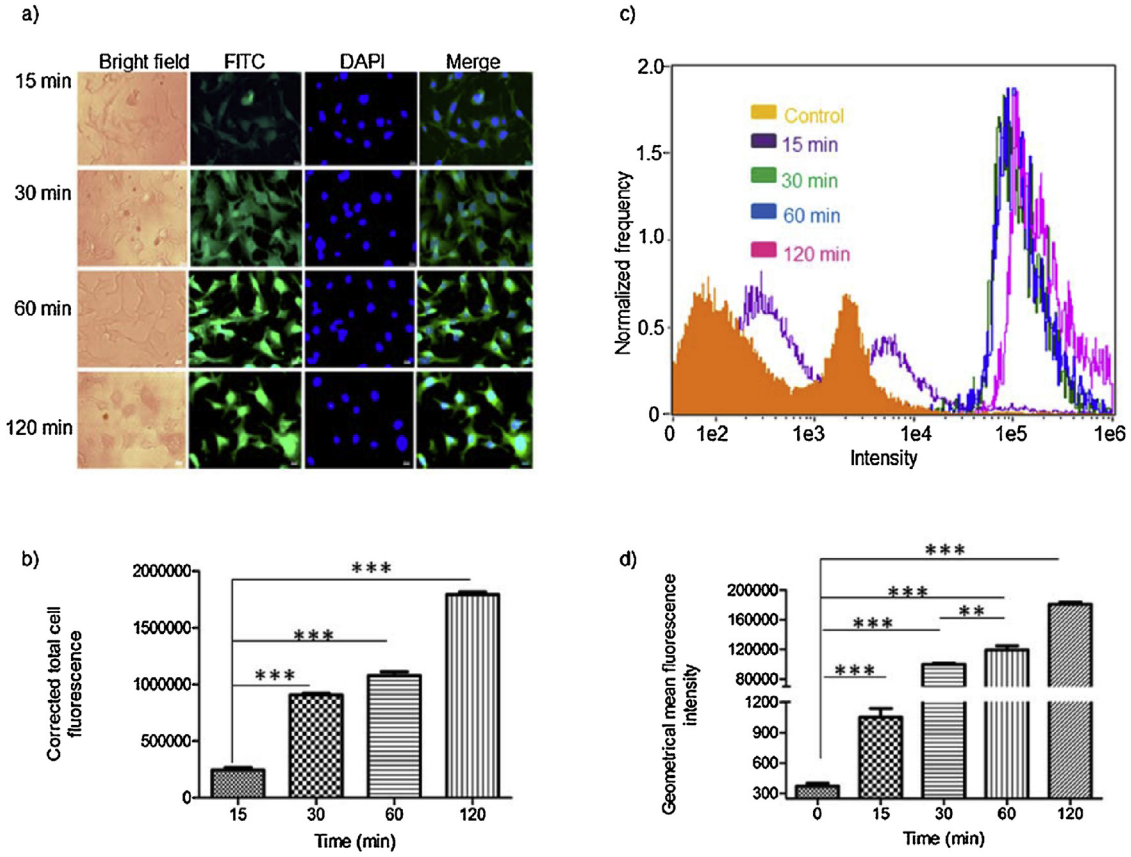

Fig. 2. (a) Cell uptake of FITC labeled AuNP-CS/SA/CS in B16F10 cancer cells after incubation for 15, 30, 60 and 120 min. Micrographs were presented in bright field, FITC filter, DAPI filter, merge of FITC and DAPI filter images. Images were representative of at least three experiments. (b) Corrected total cell fluorescence calculated through image analysis using Image J software. (c) Flow cytometry analysis of time dependent B16F10 cell uptake of AuNP-CS/SA/CS. (d) The geometric mean of fluorescence intensity obtained using Ideas software. Data represents mean ± standard deviation (n = 3). Scale bar represents 20 μm. *** and ** represents that the values are significantly different at $p < 0.001$ and $p < 0.01$, respectively.

Flow cytometric analysis showed an increase in fluorescence intensity of B16F10 cells after incubation with FITC labeled LbL-AuNP (Fig. 2c). The geometrical mean fluorescence intensity significantly ($p < 0.05$) increased with the increase in incubation time from 15 min to 120 min (Fig. 2d).

3.3. Cell uptake mechanism

To understand the LbL-AuNP cell uptake mechanism, specific endocytosis inhibitors for clathrin and caveolae mediated pathways were utilized as described in Supplementary material. There was a reduced cell uptake of FITC labeled LbL-AuNP after pretreatment with chlorpromazine rather than methyl-β-cyclodextrin compared with control cells (without inhibitor pretreatment) (Fig. 3a). The background corrected fluorescence image analysis showed a significant ($p < 0.05$) decrease in cell associated fluorescence compared to control cells (Fig. 3b). It was observed that the morphology of B16F10 cells was slightly altered after pretreatment with inhibitors. Similarly, flow cytometry showed 43% and 2% reduction in cell associated fluorescence intensity after pretreatment with chlorpromazine and methyl-β-cyclodextrin, respectively (Fig. 3c and d).

3.4. In vitro *gene silencing*

Results from Western blot analysis showed that the STAT3 expression decreased by 44.7% and 47.3% after treatment with AuNP-CS/STAT3 siRNA/CS containing 0.25 nM and 0.5 nM siRNA, respectively (Fig. 4). There was no suppression of STAT3 protein after treatment with 0.25 nM and 0.5 nM of AuNP-CS/scrambled siRNA/CS. Similarly, there was no inhibition of STAT3 protein after treatment with AuNP-CS/SA/CS containing Au concentration of 338 μM and 675 μM.

3.5. Effect of STAT3 siRNA on cell viability

Fig. 5 shows the B16F10 cell growth inhibition after treatment with free and AuNP loaded siRNA. The free siRNA at 0.5 nM did not show significant growth inhibition (2.1 ± 0.1%). The AuNP-CS/STAT3 siRNA/CS treatment resulted in 49.4 ± 0.6% and 66.2 ± 0.2% growth inhibition at 0.25 nM and 0.5 nM STAT3 siRNA concentration, respectively. The control treatment of AuNP-CS/scrambled siRNA/CS showed an inhibition of 33.0 ± 0.4% and 46.0 ± 0.1% at 0.25 nM and 0.5 nM concentration, respectively. The size control particles of AuNP-CS/SA/CS showed growth inhibition of 29.9 ± 0.9% and 37.2 ± 0.4% at 338 μM and 675 μM of Au concentration, respectively. Blank AuNP-CS showed growth inhibition of 27.8 ± 0.2 and 39.3 ± 0.6% at 338 μM and 675 μM of Au, respectively (Fig. S1).

3.6. Apoptosis assay

Fig. 6 shows percentage of cells at different stages of cell death after treatment with free and AuNP loaded siRNA. The gated cell population (10,000 cells) was divided into four quadrants as live cells, early apoptotic cells, late apoptotic cells and dead cells. A significant ($p < 0.05$) increase in the percentage of early and late apoptotic events was found after treatment with formulations con-

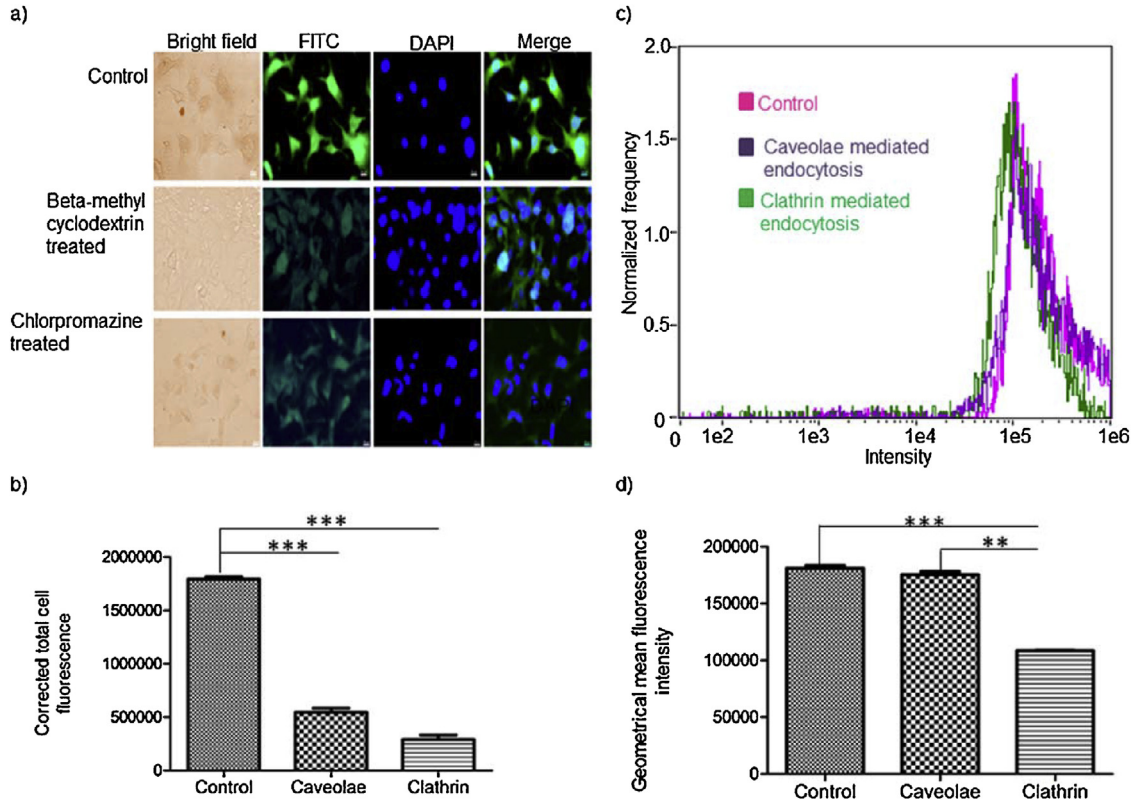

Fig. 3. (a) B16F10 cell uptake of AuNP after treatment with endocytosis inhibitors. Images were representative of at least three experiments. (b) Corrected total cell fluorescence calculated through image analysis using Image J software. (c) Flow cytometry analysis of time dependent B16F10 cell uptake of AuNP-CS/SA/CS. (d) The geometric mean of fluorescence obtained using Ideas software. Data represents mean ± standard deviation (n = 3). Scale bar represents 20 μm. *** and ** represents that the values are significantly different at $p < 0.001$ and $p < 0.01$, respectively.

taining STAT3 siRNA compared with scrambled siRNA treatment and untreated cells. Late apoptotic events of 41.90 ± 2.12% and 43.95 ± 0.21% (annexin V+/PI+) were observed after treatment with AuNP-CS/STAT3 siRNA/CS containing 0.25 nM and 0.5 nM of STAT3 siRNA. Whereas, treatment with 0.25 nM and 0.5 nM of AuNP-CS/scrambled siRNA/CS showed 1.87 ± 0.06% and 2.87 ± 0.08% late apoptotic events, respectively. Free siRNA at 0.5 nM did not show any apoptotic events. Supplementary Fig. S3 shows representative images of apoptotic cells captured using imaging flow cytometer.

3.7. Skin penetration of the LbL-AuNP

Skin penetration of the AuNP-CS/siRNA/CS was studied on excised porcine ear skin having a thickness of 0.96 ± 0.50 mm and electrical resistance of 4.34 ± 0.15 kΩ. After 4 h passive and iontophoresis application of LbL-AuNP, skin resistance decreased to 3.29 ± 0.21 kΩ and 2.03 ± 0.5 kΩ, respectively. The stability of AuNP-CS/siRNA/CS in PBS was determined for the experimental duration of 4 h using dynamic light scattering measurements. The average particle size increased to 157.5 ± 14.1 (PDI: 0.44 ± 0.08) and 229.1 ± 6.4 (PDI: 0.36 ± 0.04) from 151.8 ± 4.9 nm (PDI; 0.43 ± 0.01) after passive and anodal iontophoresis application, respectively. Whereas, zeta-potential decreased to 28.1 ± 1.2 mV and 24.7 ± 0.3 mV from 48.1 ± 1.4 mV after passive and anodal iontophoresis application. Fig. 7ashows the skin penetration of AuNP-CS/siRNA/CS after passive and iontophoresis application. Passive application of AuNP-CS/siRNA/CS did not penetrate the skin and nanoparticles were retained within the stratum corneum. It is evident that AuNP-CS/siRNA/CS was able to penetrate the stratum corneum (SC) and viable epidermis (VE) after anodal iontophoresis (Fig. 7a). Iontophoretic application promoted the skin penetration of AuNP-CS/siRNA/CS mainly through intercellular and follicular pathways (Fig. S4).

Similarly, Fig. 7b shows the confocal images of skin after passive and iontophoresis application of LbL-AuNP. Iontophoresis enhanced the skin penetration of LbL-AuNP up to 70 μm depth compared to 30 μm after passive application. Supplementary Fig. S5 shows a greater average fluorescence intensity within the skin after iontophoresis application compared with passive delivery.

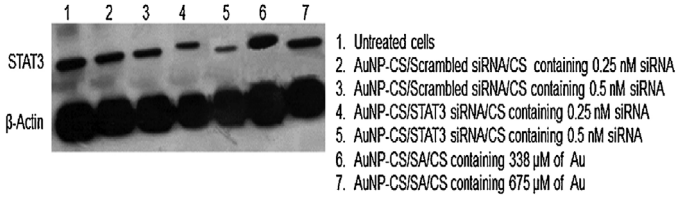

Fig. 4. Expression of STAT3 protein in B16F10 cells after treatment with STAT3 siRNA. β-actin was used as loading control.

4. Discussion

Localized delivery is expected to provide greater concentration of chemotherapeutic agents at the tumor site and avoid unwanted adverse effects [26]. Non-invasive topical delivery of anti-cancer agents shows potential to treat easily accessible skin malignancies including melanoma [27,28]. However, skin is a formidable barrier which limits the transport of active molecules. Especially, macromolecules such as siRNA with high molecular weight (13 kDa) and greater negative charge density show poor skin penetration [29]. Furthermore, naked siRNA is prone to rapid degradation in

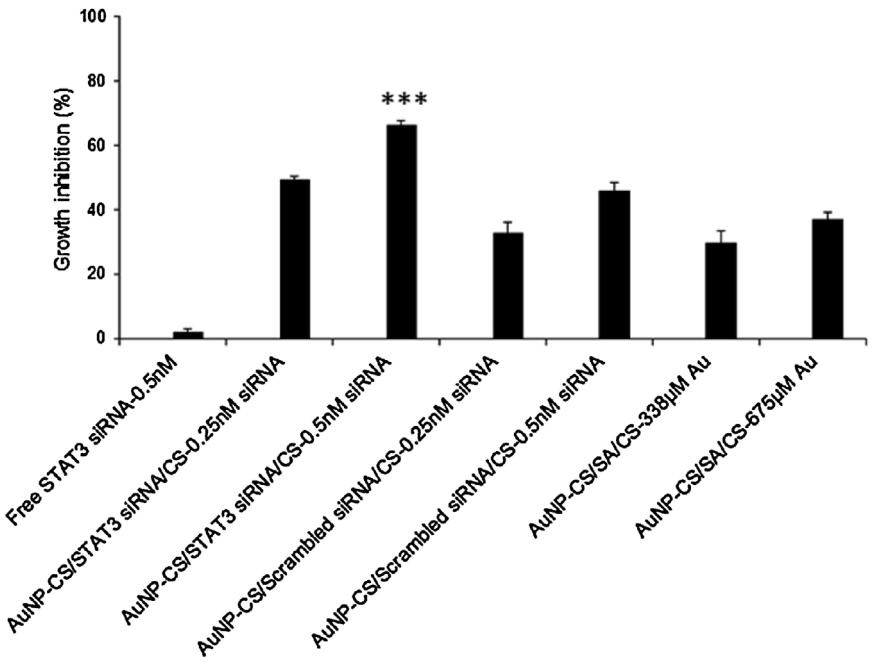

Fig. 5. Inhibition of B16F10 cancer cell growth after treatment with different concentrations of free siRNA and siRNA loaded AuNP. Data represents mean ± standard deviation (n = 3). *** represents that the value is significantly different compared with all other values at $p < 0.001$.

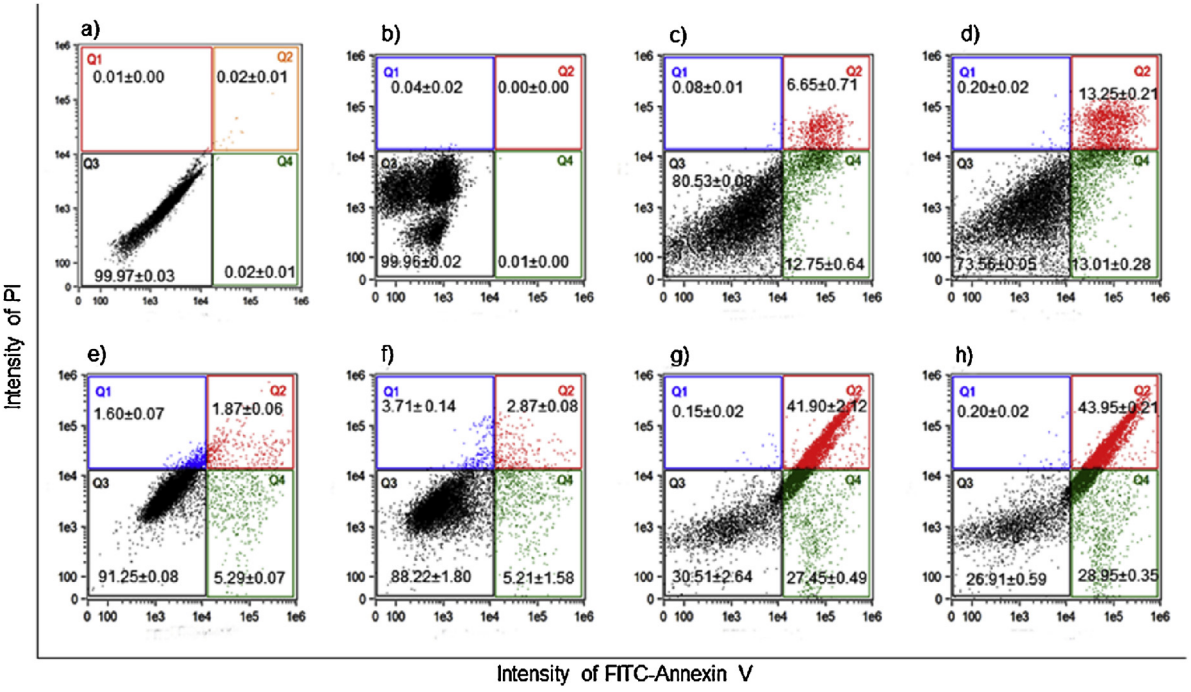

Fig. 6. Apoptosis events observed in B16F10 cells after treatment with formulations. (a) Untreated cells; (b) free STAT3 siRNA; (c & d) AuNP-CS/SA/CS containing 338 μM and 675 μM of AuNP; (e & f) AuNP-CS/scrambled-siRNA/CS at 0.25 nM and 0.5 nM; (g & h) AuNP-CS/STAT3-siRNA/CS at 0.25 nM and 0.5 nM, respectively. Dot plots are representative of three independent experiments.

biological systems. Therefore, to improve the stability and cell uptake, siRNA was entrapped in LbL-AuNP; and iontophoresis was employed to promote the localized skin penetration.

Confocal laser scanning microscope has been utilized to optically section the skin and determine the depth of penetration of fluorescent dye tagged LbL-AuNP. Similar to the earlier reports, the depth of skin penetration of nanoparticles was found to be between 50 and 100 μm in the presence of iontophoresis [27]. In other words, LbL-AuNP reached the target site of viable epidermis where melanocytes are located. The optical sectioning using confocal microscope is supported by the depth of penetration shown in skin cryosections. It was observed from the images that the primary mechanism of skin penetration is through intercellular pathways within the stratum corneum [30]. Furthermore, greater fluorescence intensity was also observed near the hair follicles (Fig. S4). Nanoparticles of particle size range between 50 and 200 nm have been shown to penetrate skin through follicular pathways [31]. In our earlier report, we have also showed that iontophoretic applica-

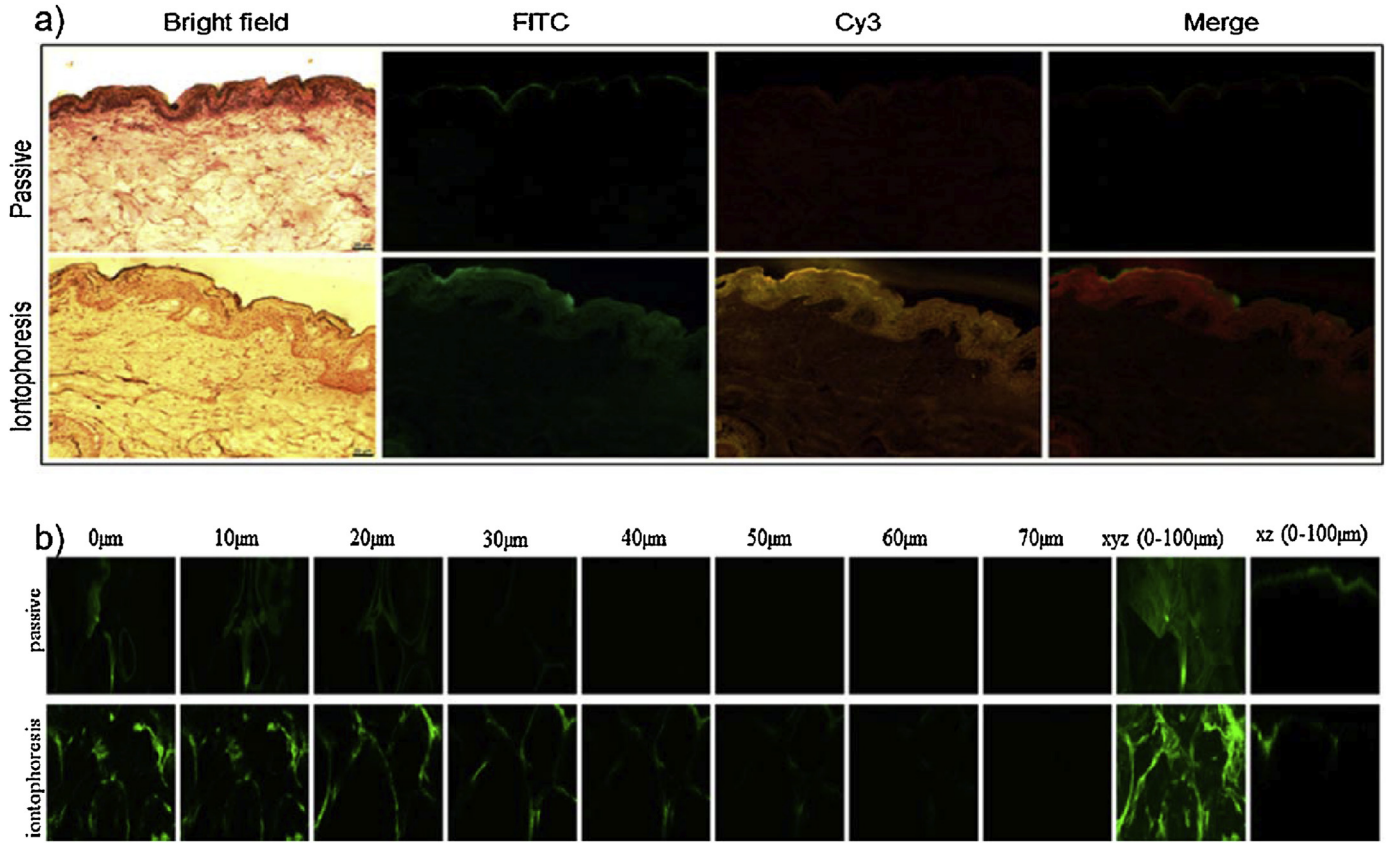

Fig. 7. (a) Skin penetration of AuNP-CS/siRNA/CS after passive and anodal iontophoresis application. Cy3 labeled siRNA and FITC labeled CS were used to construct AuNP-CS/siRNA/CS. Micrographs were presented in bright field after hematoxylin staining, FITC filter, Cy3 filter, and merge of FITC and Cy3 filter images. (b) Confocal microscopic images of skin samples after treatment with AuNP-CS/siRNA/CS for 2 h. Images were shown from surface to 70 μm depth inside skin in XYZ and XZ. All the images were representative of at least three experiments.

tion of LbL-AuNP significantly improved the deposition of imatinib mesylate in viable epidermis [20]. The LbL-AuNP and siRNA did not permeate across the skin to reach the receptor medium. Therefore, the nanoparticles were found to be localized within the skin tissue.

The ability of siRNA to silence target gene depends on its efficient cell uptake and cytoplasmic translocation [32]. In general, nanoparticles are taken-up by cells through endocytosis pathways [33]. Clathrin, caveolea and non-clathrin and non-caveolea dependent cell uptake are the predominant endocytosis mechanisms [34]. To the best knowledge of the authors, there have been no reports on the mechanism of cell-uptake of LbL-AuNP. However, the metallic AuNP have been shown to taken up by cells using clathrin-mediated endocytosis [35]. In general, the nanoparticles of size <200 nm are expected to be endocytosed through clathrin-mediated pathways, while the nanoparticles >200 nm particle size are endocytosed through caveolea-mediated pathways [36]. Furthermore, upon endocytosis, the cargo has to be released within the cytoplasm to bind to target mRNA and escape the lysosomal degradation [37]. Polyethyleneimine (PEI) has been the widely used non-viral carrier for nucleic acid delivery [38]. One of the advantages of nucleic acid complexation with PEI is rapid endosomolysis upon cell uptake attributed to proton-sponge effect. However, PEI is known to be cytotoxic [21]. In our earlier report, blank LbL-AuNP made of PEI, decreased the cell viability by 60% compared to control at 250 μM Au concentration [20]. On the other hand, chitosan is a natural polysaccharide synthesized by deacetalyzation of chitin and found to be biocompatible and biodegradable [39]. Multiple studies have compared the transfection efficiency of chitosan with that of PEI. It can be said that, while the buffering capacity and endosomolysis are weaker for chitosan based nanoparticles, the transfection efficiency is not significantly different to that of PEI [40,41]. Chitosan-plasmid DNA complexes have been shown to release from endosomes due to swelling of chitosan and endosomal rupture [42]. However, it should be noted that most of the studies where chitosan is used to deliver siRNA, chitosan is electrostatically complexed to nucleic acids through ionic gelation method. Therefore, the physical and chemical characteristics could be different from siRNA entrapped LbL-AuNP. In this study, treatment of B16F10 cells with chitosan coated AuNP resulted in 48% STAT3 protein suppression, and 44% and 29% of late and early apoptotic cells, respectively. Chitosan coated blank LbL-AuNP showed significantly lower cytotoxicity compared to PEI surfaced LbL-AuNP shown in our earlier report [20]. However, the chitosan coated blank LbL-AuNP still showed higher growth inhibition of 29.9% in B16F10 cells. The cytotoxicity of these blank nanoparticles need to be further reduced and is the subject of our ongoing research work.

Many of the oncogenic signaling pathways including receptor and non-receptor tyrosine kinases converge and transmit through STAT3 mediated pathway [43,44]. STAT3 has been identified to be activated in multiple cancer types including melanoma [43]. This activated STAT3 would enhance the cell growth and proliferation through regulation of anti-apoptotic genes Bcl-X_L, c-Myc and cyclin D1 [8]. The B16 murine melanoma cells and *in vivo* tumor specimens were reported to show enhanced STAT3 expression [10]. Melanoma cells have been shown to undergo cell death through apoptosis upon inhibition of STAT3 signaling pathway [45]. Specifically, suppression of STAT3 expression resulted in significant increase in IL-6 and caspase 3 expression, and significant decrease in VEGF level causing cell death [45]. The STAT3 protein inhibition has been shown using non-specific small molecules such as curcumin [46].

To that end, siRNA mediated STAT3 gene silencing is more specific and effective. To the best of our knowledge, this is the first time LbL-AuNP have been utilized to deliver siRNA through skin with the application of iontophoresis.

5. Conclusions

AuNP can be prepared by direct reduction of $HAuCl_4$ using chitosan. The LbL-AuNP are stable in PBS and cell culture medium for up to 48 h. siRNA can be layered on chitosan coated AuNP. Murine melanoma cells take up the siRNA loaded LbL-AuNP within 1 h predominantly through clathrin mediated pathway. The STAT3 siRNA loaded LbL-AuNP decrease the cancer cell viability through apoptosis mechanism. Furthermore, iontophoresis application enhances the skin penetration of siRNA loaded LbL-AuNP to reach viable epidermis. The LbL-AuNP penetrates the skin mainly through intercellular and follicular pathways.

Declaration

Authors declare no conflict of interest. VVKV and SL designed the studies; SL and AJ have performed the studies; VVKV and SL are involved in the data analysis and manuscript preparation.

Acknowledgements

This work was financially supported by Department of Biotechnology - Rapid Grant for Young Investigator Award (BT/PR6543/GBD/27/449/2012). Particle size analyzer and multimode plate reader were procured using a grant from Department of Science and Technology – fund for improvement of science and technology infrastructure (DST FIST).

Appendix A. Supplementary data

Supplementary data associated with this article can be found, in the online version, at http://dx.doi.org/10.1016/j.colsurfb.2016.05.076.

References

[1] J. Ferlay, I. Soerjomataram, R. Dikshit, S. Eser, C. Mathers, M. Rebelo, D.M. Parkin, D. Forman, F. Bray, Cancer incidence and mortality worldwide: sources, methods and major patterns in GLOBOCAN 2012, Int. J. Can. 136 (2015) 359–386.
[2] E. Maverakis, L.A. Cornelius, G.M. Bowen, T. Phan, F.B. Patel, S. Fitzmaurice, Y. He, B. Burrall, C. Duong, A.M. Kloxin, Metastatic melanoma–a review of current and future treatment options, Acta Derm. Venereol. 95 (2015) 516–527.
[3] J. Larkin, V. Chiarion-Sileni, R. Gonzalez, J.J. Grob, C.L. Cowey, C.D. Lao, D. Schadendorf, R. Dummer, M. Smylie, P. Rutkowski, Combined nivolumab and ipilimumab or monotherapy in untreated melanoma, N. Engl. J. Med. 373 (2015) 23–34.
[4] T. Seremet, D. Lienard, M. Suppa, A.L. Trepant, S. Rorive, E. Woff, N. Cuylits, Y. Jansen, M. Schreuer, V. Del Marmol, Successful (neo) adjuvant BRAF-targeted therapy in a patient with locally advanced BRAF V600E mutant melanoma, Melanoma Res. 25 (2015) 180–183.
[5] A. Hauschild, J.J. Grob, L.V. Demidov, T. Jouary, R. Gutzmer, M. Millward, P. Rutkowski, C.U. Blank, W.H. Miller, E. Kaempgen, Dabrafenib in BRAF-mutated metastatic melanoma: a multicentre open-label, phase 3 randomised controlled trial, Lancet 380 (2012) 358–365.
[6] P.B. Chapman, A. Hauschild, C. Robert, J.B. Haanen, P. Ascierto, J. Larkin, R. Dummer, C. Garbe, A. Testori, M. Maio, Improved survival with vemurafenib in melanoma with BRAF V600E mutation, N. Engl. J. Med. 364 (2011) 2507–2516.
[7] X. Yadav, J. Zhang, S. Liu, S. Estrem, X.-Q. Li, S. Gong, J.R. Buchanan, J.J. Henry, S.B. Starling, Peng, Reactivation of mitogen-activated protein kinase (MAPK) pathway by FGF receptor 3 (FGFR3)/Ras mediates resistance to vemurafenib in human B-RAF V600E mutant melanoma, J. Biol. Chem. 287 (2012) 28087–28098.
[8] M. Kortylewski, R. Jove, H. Yu, Targeting STAT3 affects melanoma on multiple fronts, Cancer Metastasis Rev. 24 (2005) 315–327.
[9] T. Xie, F.-J. Huang, K.D. Aldape, S.-H. Kang, M. Liu, J.E. Gershenwald, K. Xie, R. Sawaya, S. Huang, Activation of stat3 in human melanoma promotes brain metastasis, Cancer Res. 66 (2006) 3188–3196.
[10] A. Alshamsan, S. Hamdy, A. Haddadi, J. Samuel, A.O. El-Kadi, H. Uludağ, A. Lavasanifar, STAT3 knockdown in B16 melanoma by siRNA lipopolyplexes induces bystander immune response in vitro and in vivo, Transl. Oncol. 4 (2011) 178–188.
[11] A. Wittrup, J. Lieberman, Knocking down disease: a progress report on siRNA therapeutics, Nat. Rev. Genet. 16 (2015) 543–552.
[12] J. Wang, Z. Lu, M.G. Wientjes, J.L.-S. Au, Delivery of siRNA therapeutics: barriers and carriers, AAPS J. 12 (2010) 492–503.
[13] S. Zhang, B. Zhao, H. Jiang, B. Wang, B. Ma, Cationic lipids and polymers mediated vectors for delivery of siRNA, J. Controlled Release 123 (2007) 1–10.
[14] M.E. Davis, J.E. Zuckerman, C.H.J. Choi, D. Seligson, A. Tolcher, C.A. Alabi, Y. Yen, J.D. Heidel, A. Ribas, Evidence of RNAi in humans from systemically administered siRNA via targeted nanoparticles, Nature 464 (2010) 1067–1070.
[15] S. Mao, W. Sun, T. Kissel, Chitosan-based formulations for delivery of DNA and siRNA, Adv. Drug Delivery Rev. 62 (2010) 12–27.
[16] A.M. Alkilany, L.B. Thompson, S.P. Boulos, P.N. Sisco, C.J. Murphy, Gold nanorods: their potential for photothermal therapeutics and drug delivery tempered by the complexity of their biological interactions, Adv. Drug Delivery Rev. 64 (2012) 190–199.
[17] P. Scodeller, V. Flexer, R. Szamocki, E.J. Calvo, N. Tognalli, H. Troiani, A. Fainstein, Wired- enzyme core-shell Au nanoparticle biosensor, J. Am. Chem. Soc. 130 (2008) 12690–12697.
[18] W.B. Tan, Y. Zhang, Surface modification of gold and quantum dot nanoparticles with chitosan for bioapplications, J. Biomed. Mater. Res. A 75 (2005) 56–62.
[19] M. Bednarski, M. Dudek, J. Knutelska, L. Nowiński, J. Sapa, M. Zygmunt, G. Nowak, M. Luty-Błocho, M. Wojnicki, K. Fitzner, The influence of the route of administration of gold nanoparticles on their tissue distribution and basic biochemical parameters: in vivo studies, Pharmacol. Rep. 67 (2015) 405–409.
[20] S. Labala, P.K. Mandapalli, A. Kurumaddali, V.V.K. Venuganti, Layer-by-layer polymer coated gold nanoparticles for topical delivery of imatinib mesylate to treat melanoma, Mol. Pharm. 12 (2015) 878–888.
[21] C. Brunot, L. Ponsonnet, C. Lagneau, P. Farge, C. Picart, B. Grosgogeat, Cytotoxicity of polyethyleneimine (PEI), precursor base layer of polyelectrolyte multilayer films, Biomaterials 28 (2007) 632–640.
[22] M. Younes, Rinaudo, Chitin and chitosan preparation from marine sources structure, properties and applications, Mar. Drugs 13 (2015) 1133–1174.
[23] T. Kean, M. Thanou, Biodegradation, biodistribution and toxicity of chitosan, Adv. Drug Delivery Rev. 62 (2010) 3–11.
[24] S.C. Boca, M. Potara, F. Toderas, O. Stephan, P.L. Baldeck, S. Astilean, Uptake and biological effects of chitosan-capped gold nanoparticles on Chinese Hamster ovary cells, Mater. Sci. Eng. C 31 (2011) 184–189.
[25] D.R. Bhumkar, H.M. Joshi, M. Sastry, V.B. Pokharkar, Chitosan reduced gold nanoparticles as novel carriers for transmucosal delivery of insulin, Pharmacol. Res. 24 (2007) 1415–1426.
[26] J.D. Byrne, M.N. Jajja, A.T. O'Neill, L.R. Bickford, A.W. Keeler, N. Hyder, K. Wagner, A. Deal, R.E. Little, R.A. Moffitt, Local iontophoretic administration of cytotoxic therapies to solid tumors, Sci. Transl. Med. 7 (2015) 1–10.
[27] V.K. Venuganti, M. Saraswathy, C. Dwivedi, R.S. Kaushik, O.P. Perumal, Topical gene silencing by iontophoretic delivery of an antisense oligonucleotide–dendrimer nanocomplex: the proof of concept in a skin cancer mouse model, Nanoscale 7 (2015) 3903–3914.
[28] K. Kigasawa, K. Kajimoto, S. Hama, A. Saito, K. Kanamura, K. Kogure, Noninvasive delivery of siRNA into the epidermis by iontophoresis using an atopic dermatitis-like model rat, Int. J. Pharm. 383 (2010) 157–160.
[29] M. Aldawsari, M.B. Chougule, R. Jayachandra Babu, Progress in topical siRNA delivery approaches for skin disorders, Curr. Pharm. Des. 21 (2015) 4594–4605.
[30] V. Venuganti, P. Sahdev, M. Hildreth, X. Guan, O. Perumal, Structure-skin permeability relationship of dendrimers, Pharm. Res. 28 (2011) 2246–2260.
[31] T.W. Prow, J.E. Grice, L.L. Lin, R. Faye, M. Butler, W. Becker, E.M. Wurm, C. Yoong, T.A. Robertson, H.P. Soyer, Nanoparticles and microparticles for skin drug delivery, Adv. Drug Deliv. Rev. 63 (2011) 470–491.
[32] Q. Sun, Z. Kang, L. Xue, Y. Shang, Z. Su, H. Sun, Q. Ping, R. Mo, C. Zhang, A collaborative assembly strategy for tumor-targeted siRNA delivery, J. Am. Chem. Soc. 137 (2015) 6000–6010.
[33] Y. Shan, S. Ma, L. Nie, X. Shang, X. Hao, Z. Tang, H. Wang, Size-dependent endocytosis of single gold nanoparticles, Chem. Commun. 47 (2011) 8091–8093.
[34] S. Zhang, H. Gao, G. Bao, Physical principles of nanoparticle cellular endocytosis, ACS Nano 9 (2015) 8655–8671.
[35] H. Klingberg, L.B. Oddershede, K. Loeschner, E.H. Larsen, S. Loft, P. Møller, Uptake of gold nanoparticles in primary human endothelial cells, Toxicol. Res. 4 (2015) 655–666.
[36] J. Rejman, V. Oberle, I. Zuhorn, D. Hoekstra, Size-dependent internalization of particles via the pathways of clathrin-and caveolae-mediated endocytosis, Biochem. J. 377 (2004) 159–169.
[37] M.S. Shim, Y.J. Kwon, Stimuli-responsive polymers and nanomaterials for gene delivery and imaging applications, Adv. Drug Delivery Rev. 64 (2012) 1046–1059.
[38] R. Kircheis, L. Wightman, E. Wagner, Design and gene delivery activity of modified polyethylenimines, Adv. Drug Delivery Rev. 53 (2001) 341–358.

[39] W.E. Rudzinski, T.M. Aminabhavi, Chitosan as a carrier for targeted delivery of small interfering RNA, Int. J. Pharm. 399 (2010) 1–11.
[40] H.-Q. Mao, K. Roy, V.L. Troung-Le, K.A. Janes, K.Y. Lin, Y. Wang, J.T. August, K.W. Leong, Chitosan-DNA nanoparticles as gene carriers: synthesis, characterization and transfection efficiency, J. Controlled Release 70 (2001) 399–421.
[41] M. Koping-Hoggard, I. Tubulekas, H. Guan, K. Edwards, M. Nilsson, K. Varum, P. Artursson, Chitosan as a nonviral gene delivery system. Structure-property relationships and characteristics compared with polyethylenimine in vitro and after lung administration in vivo, Gene Ther. 8 (2001) 1108–1121.
[42] T. Ishii, Y. Okahata, T. Sato, Mechanism of cell transfection with plasmid/chitosan complexes, Biochim. Biophys. Acta 1514 (2001) 51–64.
[43] G. Niu, T. Bowman, M. Huang, S. Shivers, D. Reintgen, A. Daud, A. Chang, A. Kraker, R. Jove, H. Yu, Roles of activated Src and Stat3 signaling in melanoma tumor cell growth, Oncogene 21 (2002) 7001–7010.
[44] H. Yu, D. Pardoll, R. Jove, STATs in cancer inflammation and immunity: a leading role for STAT3, Nat. Rev. Cancer 9 (2009) 798–809.
[45] A. Alshamsan, S. Hamdy, J. Samuel, A.O. El-Kadi, A. Lavasanifar, H. Uludağ, The induction of tumor apoptosis in B16 melanoma following STAT3 siRNA delivery with a lipid-substituted polyethylenimine, Biomaterials 31 (2010) 1420–1428.
[46] M.A. Bill, C. Nicholas, T.A. Mace, J.P. Etter, C. Li, E.B. Schwartz, J.R. Fuchs, G.S. Young, L. Lin, J. Lin, Structurally modified curcumin analogs inhibit STAT3 phosphorylation and promote apoptosis of human renal cell carcinoma and melanoma cell lines, PLoS One 7 (2012) 407–424.